Dielectric response function and stopping power of a two-dimensional electron gas

A. Bret and C. Deutsch
Laboratoire de Physique des Gaz et des Plasmas and Groupement de Recherches, Université de Paris XI, 91405 Orsay Cedex, France
(Received 11 May 1993)

The dielectric response function of an electron gas confined in two dimensions is calculated in the random-phase approximation at any degeneracy. We then focus our attention on the stopping power of such an electron gas. The results exhibit important discrepancies with respect to the three-dimensional case. The leading term of the asymptotic expansion in the high-velocity V range is independent of the electron mass and decreases as $1/V$.

PACS number(s): 52.25.Mq, 73.20.Dx, 73.50.Bk, 73.50.Mx

I. INTRODUCTION

There is a steady interest in the two-dimensional (2D) electron gas since it has been demonstrated how to realize experimentally a 2D electron system confined to a plane with a continuously varying density. The thermodynamics of such a system has been studied by Fetter [1] and many others. The dielectric response function has been estimated in the random-phase approximation (RPA) by Stern [2] for the degenerate case ($T=0$) and by Platzman and Tzoar [3] for the classical case at high temperature. So, it remains to bridge a gap between these two extreme limits. This explains our intent to workout the RPA dielectric function at any finite temperature.

From this completed description of the 2D electron jellium, it appears of interest to derive a formulation for stopping an in-plane charged particle. This could allow for an alternative diagnostics tool for many two-dimensional electron systems of considerable interest in many fields of application. Metal-oxide semiconductor devices are a good example. This paper is thus divided into two main parts. We first evaluate the RPA dielectric response function at any degeneracy and make contact with the previous calculations [2,3] at $T=0$ and ∞, respectively. We derive a plasmon-pole approximation for the imaginary part of the inverse dielectric function which will be extensively used in the stopping power calculations. We then turn to stopping power calculations themselves, using the dielectric formalism.

Sections II and III are thus devoted to a thorough presentation of the RPA dynamic dielectric function, valid at any temperature. An efficient plasmon-pole approximation, used in the sequel, is also worked out.

These conceptual tools are then applied to the investigation of in-plane stopping for a nonrelativistic point charge, in Secs. IV and V. The high-velocity limit of the stopping power is then interpreted through the above weak-coupling limits, and a classical argumentation going back to Fermi. Low-velocity limits are also thoroughly detailed.

II. THE TWO-DIMENSIONAL ELECTRON GAS

We first recall some well-known basic properties of the 2D electron jellium. Let N electrons be confined to a surface S by a transverse potential. Neglecting their interaction we can solve the Schrödinger equation for each electron to show that its impulsion space is divided in cells of surface $(2\pi\hbar)^2/S$. Writing that, according to the Pauli principle, there can be only two electrons in each cell and that in the ground state, the energy $E=\sum_i p_i^2/2m_e$ is the smallest possible, we get

$$N=2\frac{\pi P_F^2}{(2\pi\hbar)^2/S}\ , \tag{1}$$

which means that the number of electrons is twice the number of cells within a disk of radius P_F. The above equation yields

$$P_F=\hbar(2\pi N_e)^{1/2}\ , \tag{2}$$

where $N_e=S/N$, the surface density. With $P_F=\hbar k_F$ we then get the Fermi wave vector

$$k_F=\frac{P_F}{\hbar}=(2\pi N_e)^{1/2} \tag{3}$$

and the Fermi energy

$$E_F=\frac{\hbar^2k_F^2}{2m_e}=\frac{\pi N_e\hbar^2}{m_e}\ . \tag{4}$$

At finite temperature, electrons obey the Fermi-Dirac statistics, and we can derive a relation between the chemical potential and the temperature by writing that the number dN of electrons contained in a cell is

$$dN=2\frac{d^2pS}{(2\pi\hbar)^2}\frac{1}{1+\exp\left[\dfrac{\varepsilon-\mu}{k_BT}\right]}\ , \tag{5}$$

with $\varepsilon=p^2/2m_e$ and μ is the chemical potential. As the electron number must be N we get

$$\frac{k_BT}{E_F}\int_0^\infty\frac{dx}{1+\exp(x-\alpha^e)}=1\ , \tag{6}$$

where $\alpha^e=\pi/k_BT$ is the degeneracy degree.

Setting $T_e=k_BT/E_F$ yields

$$T_e^{-1}=\ln[1+\exp(\alpha^e)]\ . \tag{7}$$

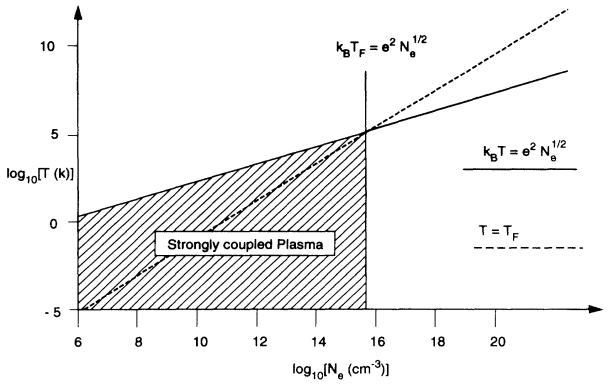

FIG. 1. Validity domain of the RPA for an electron gas confined in two dimensions. The hatched region corresponds to strongly coupled plasmas which cannot be treated within the RPA.

As we will be interested in a RPA treatment of the electron gas we now investigate the validity of the weakly coupled approximation. The various energies to be compared are the Fermi energy E_F and the electrostatic energy $e^2N_e^{1/2}$ if the gas is degenerate, while the electrostatic energy must be compared with the thermal energy k_BT in the classical case. We show in Fig. 1 the three following limits in a $\log_{10}[N_e(\mathrm{cm}^{-3})]$-$\log_{10}[T_e(\mathrm{K})]$ diagram:

$$e^2N_e^{1/2}=k_BT\ ,$$
$$E_F=k_BT\ ,$$
$$E_F=e^2N_e^{1/2}\ .$$

RPA is valid for $E_F=e^2N_e^{1/2}$ if $E_F=k_BT$ and also for $k_BT\gg e^2N_e^{1/2}$ if $E_F\ll k_BT$. In the usual experimental range of density ($10^5<N_e<10^{10}$ cm^{-2}) the gas turns classical even at a temperature ~ 10 K.

III. DIELECTRIC FUNCTION

A. General

We now introduce the longitudinal dielectric function as

$$\varepsilon(\mathbf{k},\omega)=1-V(k)\chi^0(\mathbf{k},\omega)\ , \tag{8}$$

where $V(k)$ is the two-dimensional Fourier transform on the Coulomb potential, $V(k)=2\pi e^2/k$, while $\chi^0(\mathbf{k},\omega)$ is the polarizability of the system given in the RPA by [2,3]

$$\chi^0(\mathbf{k},\omega)=\lim_{\eta\to 0}2\int\int\frac{d^2q}{(2\pi)^2}\frac{n^0(\mathbf{q}+\mathbf{k})-n^0(\mathbf{q})}{\varepsilon^0_{\mathbf{q}+\mathbf{k}}-\varepsilon^0_{\mathbf{q}}-\hbar\omega-i\eta}\ , \tag{9}$$

$n^0(\mathbf{q})$ being the Fermi-Dirac statistics and $\varepsilon^0_{\mathbf{k}}=\hbar^2k^2/2m_e$. We now introduce the usual Lindhard dimensionless quantities previously used by Gouédard and Deutsch [4] in a similar calculation for the three-dimensional case

$$K=\frac{k}{k_F},\quad Q=\frac{q}{k_f},\quad \nu=\frac{\hbar\omega}{E_F},\quad \gamma=\frac{\mu}{E_f},\quad T_e=\frac{k_BT}{E_F}\ . \tag{10}$$

We thus obtain

$$n^0(\mathbf{q})=n^0(\mathbf{Q})=\frac{1}{1+\exp\left[\dfrac{Q^2-\gamma}{T_e}\right]}\ , \tag{11}$$

and

$$\chi^0(\mathbf{k},\omega)=\lim_{\eta\to 0}2\frac{k_F^2}{E_F}\int\int\frac{d^2Q}{(2\pi)^2}\frac{n^0(\mathbf{Q}+\mathbf{k})-n^0(\mathbf{Q})}{(\mathbf{Q}+\mathbf{K})^2-(\mathbf{Q})^2-\nu-i\eta}\ . \tag{12}$$

Separating the quadrature in two parts we have

$$\chi^0(\mathbf{k},\omega)=\frac{2k_F^2}{(2\pi)^2E_F}\frac{1}{2K}[f(p_-)-f(p_+)] \tag{13}$$

with $p_\pm=\nu/2K\pm K/2$ and

$$f(x)=\lim_{\eta'\to 0}\int_0^\infty Qn^0(Q)dQ\int_0^{2\pi}\frac{d\theta}{x-Q\cos\theta+i\eta'}\ , \tag{14}$$

where $\eta'=\eta/2K$. The calculation explained in Appendix A yields

$$f(x)=2\pi\frac{x}{|x|}\int_0^x\frac{Qn^0(Q)dQ}{\sqrt{x^2-Q^2}}-\int_x^\infty\frac{Qn^0(Q)dQ}{\sqrt{Q^2-x^2}}\ . \tag{15}$$

It is worth noticing that $p_\pm=u\pm z$, while u and z are the usual Lindhard variables of the 3D problem. We finally get an expression for the polarizability close to the 3D one,

$$\varepsilon(z,u)=1-\frac{\chi^2}{4z^2}[f(u-z)-f(u+z)]\ ,$$
$$\chi^2=\frac{1}{\pi k_Fa_0},\quad z=\frac{k}{2k_F},\quad u=\frac{\omega}{kV_F}\ , \tag{16}$$

where a_0 is the Bohr radius.

B. Dispersion relation

We now solve approximately the equation $\mathrm{Re}[\varepsilon(z_r,u_r)]=0$ for $z\ll 1$ and $u\gg 1$. We first get an asymptotic expansion of $\mathrm{Re}[f(u-z)-f(u+z)]$ with

$$\mathrm{Re}[f(u-z)-f(u+z)]\approx\frac{2\pi z}{u^2}\sum_{k=0}^{\infty}a_kF(k)(\alpha^e)T_e^k\frac{2k+1}{u^{2k}} \tag{17}$$

$F_k(\alpha^e)$ being the kth Fermi function,

$$F_k(\alpha^e)=\int_0^\infty\frac{x^kdx}{1+\exp(x-\alpha^e)}\ , \tag{18}$$

while the a_k's come from $(1-x)^{-1/2}=\sum_{k=0}^{\infty}a_kx^k$ so that $a_0=1,a_1=\frac{1}{2},a_3=\frac{3}{8},\ldots$. The dispersion relation then reads as

$$z_r=\frac{\pi\chi^2}{2u_r^2}\left[1+\frac{3}{2}T_e^2\frac{F_1(\alpha^e)}{u_r^2}+\frac{15}{8}T_e^4\frac{F_2(\alpha^e)}{u_r^4}+\cdots\right], \tag{19}$$

where we made use of Eq. (7), $F_0(\alpha^e)T_e=1$. If we restrict Eq. (19) to lowest order we get

$$\omega_p^2(k)=\frac{2\pi N_e e^2}{m_e}k , \tag{20}$$

a result already obtained by many authors (see [1–3,5]) showing that the plasma frequency in the 2D case is k dependent.

C. Limit behaviors

We now investigate the $T=0$ limit of the dielectric function. In the calculation on the function $f(x)$ defined in Eq. (15), we then set $n^0(Q)=1$ for $Q<1$ and $n^0(Q)=0$ for $Q>1$ so that

$$f(x)=2\pi\begin{cases}x-i\sqrt{x^2-1} & \text{if } |x|>1\\ x-\dfrac{x}{|x|}\sqrt{1-x^2} & \text{otherwise,}\end{cases} \tag{21}$$

which is the result already obtained by Stern [2].

When the parameter T_e tends to infinity, Eq. (7) shows that $\exp(\alpha_e)\approx 1/T_e$ and we get

$$f(x)\approx\frac{2\pi\exp(-x^2/T_e)}{\sqrt{T_e}}\left[\Phi(x/\sqrt{T_e})-i\frac{\sqrt{\pi}}{2}\right], \tag{22}$$

with $\Phi(u)=\int_0^u e^{t^2}dt$. We here define some additional dimensionless quantities ($V_{\rm th}$ is the thermal velocity),

$$U=\frac{u}{T_e^{1/2}}=\frac{\omega}{k_B V_{\rm th}},\quad Z=\frac{z}{T_e^{1/2}}=\frac{k\lambda}{2} , \tag{23}$$

with $\frac{1}{2}m_e V_{\rm th}^2=k_B T$ and $\lambda=\hbar/m_e V_{\rm th}$, the classical electron de Broglie length. In the classical limit ($T_e\to 0$ or $\hbar\to 0$), U remains fixed while $Z\to 0$ so one has

$$\varepsilon(z,U)=1+\frac{K}{z}\left[1-2Ue^{-U^2}\Phi(U)+i\frac{\sqrt{\pi}}{2}Ue^{-U^2}\right], \tag{24}$$

reminiscent of the 3D Fried-Conte expressions [4], where

$$z=\frac{k}{2k_F},\quad U=\frac{\omega}{kV_{\rm th}},\quad K=\frac{\pi\chi^2}{2T_e}=\left[\frac{\pi}{8}\right]^{1/2}\frac{N_e^{1/2}e^2}{k_B T} , \tag{25}$$

which is the result of Platzman and Tzoar [3].

D. Sum rule

For N electrons confined in surface S, one has [6]

$$\int_{-\infty}^{\infty}(1/\varepsilon-1)\omega\,d\omega=i\pi\frac{V(k)}{S}\langle\Psi^0|[[H,\rho_{-k}],\rho_k]|\Psi^0\rangle , \tag{26}$$

$V(k)$ being the Fourier transform of the Coulomb potential, ρ_k the Fourier transform of the density operator, $|\Psi^0\rangle$ the unperturbed ground state (here, the perturbation is the Coulomb potential), and

$$H=\sum_i\frac{p_i^2}{2m_e}+\frac{1}{2}\sum_{i\neq j}V(\mathbf{r}_i-\mathbf{r}_j) . \tag{27}$$

Whatever the dimension, one finds [6]

$$[[H,\rho_{-k}],\rho_k]=-\frac{Nk^2}{m_e} . \tag{28}$$

Because the Fourier transform of the Coulomb potential is performed in two dimensions, Eq. (26) yields

$$\int_{-\infty}^{\infty}(1/\varepsilon-1)\omega\,d\omega=-i\pi\frac{2\pi e^2N_e}{m_e}k . \tag{29}$$

Taking the imaginary part of both sides and introducing

$$\omega_p^2(k)=\frac{2\pi e^2N_e}{m_e}k ,$$

a useful sum rule satisfied by the imaginary part of the inverse dielectric function is found to be

$$\int_0^{\infty}\omega\,\mathrm{Im}\left[\frac{-1}{\varepsilon(k,\omega)}\right]d\omega=\frac{\pi}{2}\omega_p^2(k) . \tag{30}$$

In term of the variables z and u, this reads as

$$\int_0^{\infty}\omega\,\mathrm{Im}\left[\frac{-1}{\varepsilon(z,u)}\right]d\omega=\frac{\pi^2\chi^2}{4z} . \tag{31}$$

E. Analytical properties

We now investigate some analytical properties of the imaginary part of the inverse dielectric function in order to prepare our stopping power study.

Behavior at $T=0$. The calculations of Stern [2] show that, as for the three-dimensional case [7], the function $\mathrm{Im}[1/\varepsilon(z,u)]$ takes significant values essentially on two regions in the plane (z,u): (i) on the resonance curve $z_r=\pi\chi^2/2u_r^2$ which corresponds to plasmon excitation; (ii) in the region $|z-u|<1$ which pertains to electron-hole excitation. It can be seen that there cannot be any electron-hole excitation outside the zone $|z-u|<1$ because the Fermi-Dirac statistics falls to 0 outside the Fermi disk if the system is in its ground state.

Behavior at T finite. When the temperature departs from 0 the resonance curve is slightly changed [see Eq. (19)], but some electrons escape from the Fermi disk. The function $\mathrm{Im}[1/\varepsilon(z,u)]$ then departs from 0 outside the region $|z-u|<1$. But since the classical distribution function falls exponentially to zero for velocities greater than thermal velocity there will be very few electron-hole excitations outside the domain $|z-u|<V_{\rm th}/V_F$. This can be seen mathematically on the imaginary part of the function f defined in Eq. (15). In the classical approximation we may write [see Eq. (22)]

$$\mathrm{Im}[f(x)] \approx -\frac{\pi^{3/2}}{T_e^{1/2}} \exp\left[-\frac{x^2}{T_e}\right], \tag{32}$$

which strongly decreases as soon as $x > T_e^{1/2}$ and it is easily checked out that $T_e^{1/2} = V_{\mathrm{th}}/V_F$ in the classical case. Therefore, we introduce as in the 3D case [4] the quantity

$$A_0(T_e) = \frac{V_e}{V_F}, \tag{33}$$

where V_e will be the average electron velocity at any temperature; $V_e = V_F$ at $T = 0$ while $V_e = V_{\mathrm{th}}$ in the classical case.

We display in Fig. 2 the domain of the function $\mathrm{Im}[1/\varepsilon]$ for any temperature with the two regions: $|z-u| < A_0/(T_e)$ for electron-hole excitations and the resonance curve for plasmons excitations. It can be shown [5] that the resonance curve does not penetrate the continuum of electron-hole excitations.

We finally set up a plasmon-pole approximation for $\mathrm{Im}[1/\varepsilon]$ in the same fashion as in the 3D case [8]. We concentrate all the intensity of the function on the resonance curve and on the line $z = u$ and make sure that the sum rule (31) is satisfied. We thus get

$$\mathrm{Im}\left[\frac{-1}{\varepsilon(z,u)}\right] \approx \frac{\pi^2\chi^2}{4uz}\left[Y(Z_1 - z)\delta\left[z - \frac{\pi\chi^2}{2u^2}\right] + Y(z - Z_1)\delta(z-u)\right], \tag{34}$$

δ being the Dirac distribution, Y the Heaviside function, and

$$Z_1 = \frac{\pi\chi^2}{2A_0^2(T_e)}, \tag{35}$$

so that Z_1 is the highest value of z pertaining to the resonance curve (see Fig. 2).

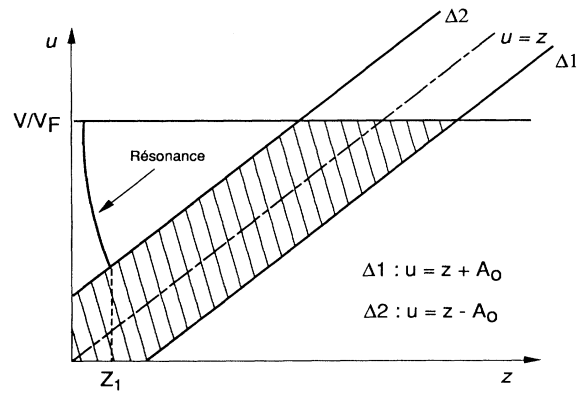

FIG. 2. Domain of importance of the imaginary part of the inverse dielectric function. The shaded area pertains to electron-hole excitations while the solid curve indicates the resonance. We also figure the integration domain used in the stopping power calculations with $0 < z < \infty$ and $0 < u < V/F_F$.

IV. STOPPING POWER

A. General

We now turn to the stopping power. If an ion of charge Z penetrates the confined electron gas with a velocity $\mathbf{V}$ included in the confinement plane it will be confined as well and can be described by a surface charge density $Ze\delta(\mathbf{r} - \mathbf{V}t)$. More generally, if the ion is no longer considered as pointlike or we introduce a dicluster, the charge distribution penetrating the electron gas should be written as $\sigma(\mathbf{r} - \mathbf{V}t)$.

To calculate the stopping power, we use the dielectric formalism, neglecting any Barkas effect by assuming that the projectile is a small perturbation in the medium. We also assume a straight-line trajectory for the charge distribution, which means that its kinetic energy must be greater than the average kinetic energy in the electron gas. The stopping power for the distribution penetrating the 2D electron gas is then calculated as in the 3D case [9]. First, the Fourier component of the field induced in the medium by the charge perturbation is given in the dielectric formalism by

$$\mathbf{E}(\mathbf{k},\omega) = -2i\pi\frac{\mathbf{k}}{k}\frac{\sigma(\mathbf{k})\delta(\omega - \mathbf{k}\cdot\mathbf{V})}{\varepsilon(k,\omega)}, \tag{36}$$

$\sigma(\mathbf{k})$ being the Fourier transform of the charge distribution $\sigma(\mathbf{r})$ at rest, setting $\sigma(\mathbf{r}) = Ze\delta(r)$ for a pointlike charge yields $\sigma(\mathbf{k}) = Ze$. The energy loss per unit path length is then (see [9])

$$-\frac{dE}{dx} = \frac{1}{2\pi V}\int\int d^2k \frac{\mathbf{k}\cdot\mathbf{V}}{k}\,\mathrm{Im}\left[\frac{-1}{\varepsilon(\mathbf{k},\mathbf{k}\cdot\mathbf{V})}\right]|\sigma(\mathbf{k})|^2 . \tag{37}$$

We now assume a spherically symmetry charge distribution with $\sigma(\mathbf{r}) = \sigma(\mathbf{r})$ and $\sigma(\mathbf{k}) = \sigma(k)$. The above equation then simplifies into

$$-\frac{dE}{dx} = \frac{1}{2\pi V}\int_0^\infty dk|\sigma(k)|^2 \int_0^{kV} \frac{\omega\, d\omega}{\sqrt{k^2V^2 - \omega^2}} \times \mathrm{Im}\left[\frac{-1}{\varepsilon(k,\omega)}\right]. \tag{38}$$

We restrict for now the calculations to a pointlike ion, so we set $|\sigma(k)|^2 = (Ze)^2$ in Eq. (38). We then express the quadrature in term of the dimensionless variables z and u and formulate the stopping power as it is usually done in the 3D calculation [10] as

$$-\frac{dE}{dx} = \frac{4}{3}\frac{Z^2e^4}{\pi m_e V^2}k_F^3 L, \tag{39}$$

with

$$L = \frac{6}{\pi\chi^2}\int_0^\infty z\, dz \int_0^{V/V_F} \frac{u\, du}{\sqrt{1 - u^2V_F^2/V^2}}\,\mathrm{Im}\left[\frac{-1}{\varepsilon(z,u)}\right]. \tag{40}$$

We can investigate some qualitative differences between the 2D and the 3D case. It is well known that in

the 3D case, the stopping power arises equally from plasmons and electron-hole excitations in the medium [7]. In both the 2D and the 3D case, the ion loses an energy quantum $\hbar\omega=\hbar\omega_p$ through a plasmon excitation. Such excitations occurring at low k (or low z) in both cases, the energy loss is lower in the 2D case because the plasma frequency behaves as $\sqrt{k}$ [see Eq. (20)]. As far as the electron-hole excitations are concerned, Eq. (40) shows that they are emphasized through the factor $\sqrt{1-u^2V_F^2/V^2}$ in the denominator. Finally, though the stopping power mechanism appears analogous to the 3D one, the ion penetrating the gas is no longer equally stopped by plasmons and electron-hole excitations but mostly by electron-hole excitations. We now turn to the calculation of the stopping power.

B. High-velocity range

We here look for the leading term of the asymptotic expansion of L given by Eq. (40) when $V/V_F \gg 1$. We perform the calculation at $T=0$ expecting that, as in the 3D case [10], the leading term does not depend on the temperature. We then make use of the plasmon-pole approximation (34) to compute L. We split L into its plasmons and electron-hole excitations parts and write

$$L=L_p+L_{e\text{-}h}$$

(subscripts p and e-h stand for plasmons and electron-hole) with

$$L_p=\frac{3\pi}{2}\int_{Z_0}^{Z_1}\frac{dz}{[1-u_r^2(z)V_F^2/V^2]^{1/2}}$$

and

$$L_{e\text{-}h}=\frac{3\pi}{2}\int_{Z_1}^{V/V_F}\frac{dz}{(1-z^2V_F^2/V^2)^{1/2}} \approx\frac{3\pi^2}{4}\left[\frac{V}{V_F}-\chi^2\right], \tag{41}$$

where (see with Fig. 2)

$$u_r^2(z)=\frac{\pi\chi^2}{2z},\quad Z_0=\frac{\pi\chi^2}{2(V/V_F)^2},\quad Z_1=\frac{\pi\chi^2}{2}.$$

L_p can be rewritten under the form

$$L_p=\frac{3\pi^2\chi^2}{4}H(V/V_F), \tag{42}$$

where

$$H(x)=Y(x-1)\frac{1}{x^2}\int_{1/x^2}^{1}\frac{dt}{t^2}\frac{1}{\sqrt{1-t}}, \tag{43}$$

where Y is the Heaviside function preventing the plasmon stopping power from departing from 0 when $V/V_F<1$ since there are no plasmon excitations in the low-velocity range. We plot in Fig. 3 the function $H(x)$. This function tends to 1 when x tends to infinity and reaches a maximum near $x\approx 1.8$. As previously noticed, the stopping power through plasmon excitations is negligible compared to the electron-hole excitations contribution which increases continuously with the velocity [see Eq. (41)]. We then obtain for the asymptotic expansion of L,

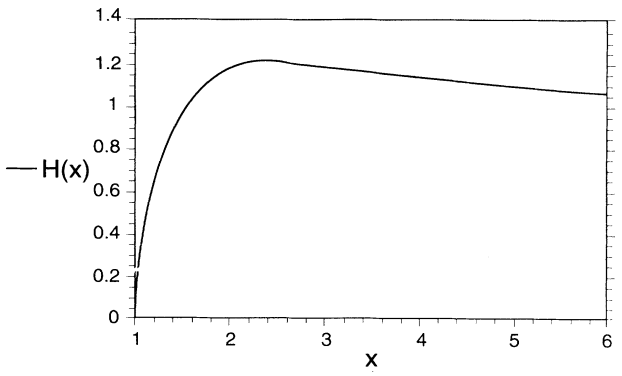

FIG. 3. Plot of the function $H(x)$ defined by Eq. (43) entering the calculation of the plasmons stopping power at high velocity. $H(x)$ reaches a maximum for $x\approx 1.8$ and tends to 1 as x tends to ∞. $H(x<1)=0$.

$$L=\frac{3\pi^2}{4}\frac{V}{V_F}+O(1). \tag{44}$$

Let us recall the 3D result (see [7]),

$$L^{3D}=\ln\left[\frac{2m_eV^2}{\hbar\omega_p}\right]+O(1). \tag{45}$$

Inserting the result (44) into Eq. (39) we derive

$$-\frac{dE}{dx}=2\pi^2\frac{Z^2e^4N_e}{\hbar V}+O\left[\frac{1}{V^2}\right], \tag{46}$$

which does not contain the gas electron mass m_e anymore; m_e appears only in the higher terms of the expansion. The other main discrepancy between the 2D and the 3D result is that the stopping power falls as $1/V$ instead as $\ln(V)/V^2$ in the 3D case. We compare in Fig. 4 the numerical evaluation of the quadrature (40) where we use Stern's dielectric function at $T=0$ [see Eq. (21) or [2]] with the expression (44) in term of the parameter V/V_F. In order to check the m_e independence of our result we performed three numerical evaluations of (40).

We first injected the true electron mass in the computation, then we performed the computation with $50m_e$ and $100m_e$, respectively. One can notice in Fig. 4 that numerical results depart only slightly from analytical ones even for $100m_e$. Anyway, it appears that the leading term of the asymptotic expansion of L actually does not depend on m_e since an increased electron mass does not affect the slope of the curve. Some more detailed calculations show that the next term of the asymptotic expansion is roughly proportional to the electron mass so that decreasing it just makes the analytic formula (44) more accurate.

Equation (46) exhibits an intrinsically quantum behavior through its $\hbar^{-1}$ dependence, already displayed by other 2D equilibrium quantities [11,12]. However, it

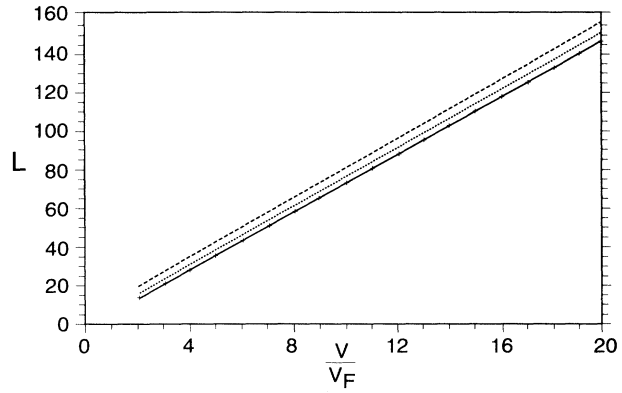

FIG. 4. Comparison between the analytic formula given by Eq. (44) and numerical evaluation of quadrature (40) using Stern's [2] dielectric function at $T=0$ and increasing electron masses. +: analytic formula (44). Solid line: numerical evaluation computed with the physical electron mass m_e. Short-dashed line: numerical evaluation computed with an electron mass equal to $50m_e$. Long-dashed line: numerical evaluation computed with an electron mass equal to $100m_e$. All curves are plotted in terms of V/V_F.

should be appreciated that despite their very different high-V behavior, Eqs. (45) and (46) may be retrieved through similar classical arguments. The initial 3D line of reasoning due to Fermi [13] may be straightforwardly extended to the present case, as follows. For this purpose, let us then focus attention on the linear ion trajectory in 2D jellium. By simply symmetry considerations, the most efficient ion stopping will arise from the electrons located transversely to the instantaneous projectile position, say at a distance b.

The energy exchanged in one collision is then obviously

$$\Delta E=\frac{(\Delta p)^2}{2m_e}=\left[\frac{ze^2}{b^2}\right]^2\frac{b^2}{V^2}\frac{1}{2m_e}\ .$$

Taking the average over every available target electron provides the mean energy loss

$$\langle\Delta E\rangle=\frac{(ze^2)^2}{2m_eV^2}N_e2\int_{b_{\min}}^{b_{\max}}\frac{db}{b^2}\ ,$$

which through $b_{\max}\gg b_{\min}=\hbar/2m_eV$ yields the first term in the right-hand side of Eq. (46) within prefactor π^2. Fermi's derivations in three dimensions reproduces exactly the Bethe result (45), because it is then possible to make use of the Gauss theorem relating projectile electric field and charge. This is not the case for electrons confined within a plane. Nevertheless, apart from this π^2 constant, all the basic physics is retrieved.

C. Low-velocity range

We now turn to the calculation of the stopping power when the ion velocity is less than the average electron velocity in the jellium. Since we considered a straight-line trajectory for the projectile, the following condition must be fulfilled:

$$\frac{1}{2}MV^2\gg\frac{1}{2}m_eV_e^2\Longleftrightarrow V\gg\left[\frac{m_e}{M}\right]^{1/2}V_e\ , \tag{47}$$

M,V being the ion mass and velocity. As we are interested in ion energy loss, the smallness of the quantity $\sqrt{m_e/M}$ shows us that we are allowed to investigate some low-velocity effects as long as the above condition is fulfilled.

To proceed with the calculation we express the dielectric function as

$$\varepsilon(z,u)=1-\frac{\chi^2}{4Z^2}[f_1(z,u)+if_2(z,u)]\ , \tag{48}$$

with

$$f_1(z,u)=2\pi D_-\int_0^{u-z}\frac{kn^0(k)dk}{\sqrt{(u-z)^2-k^2}}-2\pi D_+\int_0^{u+z}\frac{kn^0(k)dk}{\sqrt{(u+z)^2-k^2}}\ , \tag{49}$$

$$f_2(z,u)=2\pi\int_{u-z}^{\infty}\frac{kn^0(k)dk}{\sqrt{k^2-(u-z)^2}}-2\pi\int_{u+z}^{\infty}\frac{kn^0(k)dk}{\sqrt{k^2-(u+z)^2}}\ , \tag{50}$$

where

$$D_{\pm}=\frac{|z\pm u|}{z\pm u}\ . \tag{51}$$

Thus we get

$$\mathrm{Im}\left[\frac{-1}{\varepsilon(z,u)}\right]=\frac{-4z^2\chi^2f_2(z,u)}{\{4z^2-\chi^2f_1(z,u)\}^2-\{\chi^2f_2(z,u)\}^2}\ . \tag{52}$$

When $V/V_e\ll1$, we follow the 3D treatment [7,10]. We approximate the function $\mathrm{Im}(1/\varepsilon)$ in the integrand of Eq. (40) taking $f_1(z,u)\approx f_1(z,0)$ and $f_2(z,u)\approx u(\partial f_2/\partial u)_{u=0}$. To simplify the matter further we make use of $f_2(z,0)=0$ in the denominator of Eq. (52). So, we have

$$L=\frac{3}{8}\left[\frac{V}{V_F}\right]^3\int_0^{\infty}\frac{-z\left[\frac{\partial f_2}{\partial u}\right]_{u=0}dz}{[z-\chi^2f_1(z,0)/4z]^2}\ . \tag{53}$$

We find that L is proportional to V^3 so that, according to Eq. (39), the stopping power becomes proportional to the velocity as in three dimensions. It is worth noticing that the quantity $z-\chi^2f_1(z,0)/4z$ in Eq. (53) displays the static screening. We derive in Appendix B the following relation:

$$z-\frac{\chi^2}{4z}f_1(z,0)\approx\frac{k}{2k_F}+\frac{\pi\chi^2}{1+\exp(-\alpha^e)},\quad z\to0\ . \tag{54}$$

In a classical gas ($T_e\gg1$); making use of Eq. (7) we find

$$\frac{\pi\chi^2}{1+\exp(-\alpha^e)} \approx \frac{k_D}{2k_F} , \tag{55}$$

where

$$k_D^{-1} = \frac{k_B T}{2\pi N_e e^2} \tag{56}$$

is the 2D analog of the 3D Debye static screening length [1] while in the degenerate case ($T_e \ll 1$) one has

$$\frac{\pi\chi^2}{1+\exp(-\alpha^e)} \approx \frac{a_0^{-1}}{k_F} , \tag{57}$$

where a_0 is the Bohr radius and the static screening length in the degenerate 2D electron gas [5].

We can derive some equivalents of Eq. (53) in the classical and degenerate cases: when $T_e \gg 1$, Eq. (53) simplifies into

$$L = \frac{3\pi^{3/2}}{2T_e} \left[\frac{V}{V_F} \right]^3 \int_0^\infty \frac{x^2 e^{-x^2} dx}{\left[x - \frac{x^2 f_1(x\sqrt{T_e},0)}{4xT_e} \right]^2} . \tag{58}$$

We now substitute [10]

$$-\frac{\chi^2 f_1(x\sqrt{T_e},0)}{4x\sqrt{T_e},0} \leftrightarrow \lim_{x\to 0} -\frac{\chi^2 f_1(x\sqrt{T_e},0)}{4x\sqrt{T_e},0} = \frac{k_D}{2k_F} \tag{59}$$

which produces

$$L = \frac{3\pi^{3/2}}{2T_e} \left[\frac{V}{V_F} \right]^3 \Phi(A) \tag{60}$$

with

$$\Phi(A) = \int_0^\infty \frac{u^2 e^{-u^2} du}{(u+A)^2} \tag{61}$$

and A as

$$A = \frac{k_D}{2k_F T_e^{1/2}} = \left[\frac{2\pi}{T_e} \right]^{1/2} \frac{N_e^{1/2} e^2}{k_B T} . \tag{62}$$

In the present study we can restrict to $A \ll 1$, as evidenced by Fig. 5 for Φ in term of A varying from 0 to 1. Finally L can be roughly evaluated by setting $\Phi(A) \approx \Phi(0) = \sqrt{\pi/2}$ in Eq. (60) with

$$L \approx \frac{3\pi^2}{4T_e} \left[\frac{V}{V_F} \right]^3 . \tag{63}$$

When $T=0$ we get

$$L_{T=0} = \frac{3\pi}{4} \left[\frac{V}{V_F} \right]^3 G(\chi^2) , \tag{64}$$

where

$$G(\chi^2) = \int_0^1 \frac{z^2 dz}{\sqrt{1-z^2}[z - \chi^2 f_1(z,0)/4z]^2} . \tag{65}$$

We plot in Fig. 5 the function $G(\chi^2)$ for χ^2 varying from 0 to 1 since our study deals with an RPA gas where $\chi^2 \ll 1$. One can then set $G(\chi^2) \approx G(0) = \pi/2$ to obtain

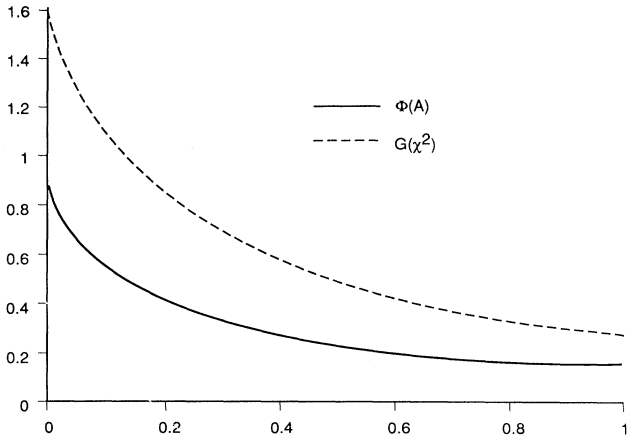

FIG. 5. Functions $\Phi(A)$ given by Eq. (61) and $G(\chi^2)$ given by Eq. (65), both dealing with the stopping power in the low-velocity range and plotted for A and χ^2 varying from 0 to 1. One has $\Phi(0) = \sqrt{\pi/2}$ and $G(0) = \pi/2$.

$$L_{T=0} \approx \frac{3\pi^2}{8} \left[\frac{V}{V_F} \right]^3 . \tag{66}$$

D. A few numerical applications

We provide now the evaluation of some formulas involved in the present paper. The stopping power at high velocity given in Eq. (46) reads as

$$-\frac{dE}{dx} = 3.47\times 10^8 \frac{Z^2 N_e M^{1/2}}{E^{1/2}} \text{ eV/cm} . \tag{67}$$

with N_e in cm^{-2}, M (ion mass) in g, and the ion energy E in eV. The leading term of the stopping distance D can be evaluated as

$$D = \int_{E_i}^{E_i/10} \frac{dE}{\left[\frac{dE}{dx} \right]} , \tag{68}$$

where E_i is the initial energy of the ion and dE/dx is given by Eq. (46) if we assume that the ion velocity is still greater than V_e when it has lost 90% of its initial energy. We thus have

$$D \approx \frac{1.88\times 10^{-9}}{Z^2 N_e M^{1/2}} E_i^{3/2} \text{ cm} . \tag{69}$$

Considering a proton penetrating a two-dimensional electron gas with a density $N_e = 10^8$ cm^{-2} with an initial energy $E_i = 10$ keV we find

$$\left[\frac{dE}{dx} \right]_{E=E_i} \approx 0.32 \text{ keV/cm}$$

and

$$D \approx 15 \text{ cm} .$$

We finally give numerical expressions for the average kinetic energy in the gas. In the classical case, this kinetic energy is given by $k_B T$ while in the degenerate case it corresponds to the Fermi energy

$$E_F=\frac{\pi N_e \hbar^2}{m_e}=2.4\times 10^{-15} N_e \text{ eV} , \tag{70}$$

with N_e in cm^{-2} so that $N_e=10^{16}$ cm^{-2} yields $E_F=24$ eV.

V. CONCLUSION

We have obtained the dielectric response function of a two-dimensional electron gas in the random-phase approximation at any degeneracy, bridging a gap between the previous calculations of Stern [2] on one hand and Platzman and Tzoar [3] on the other. We have then calculated the stopping power of such a system using the dielectric formalism. The high-velocity range asymptotic expansion is found to decrease as $1/V$ [instead of $\ln(V)/V^2$ in the 3D case] and to be independent of the electron mass. The calculations of the last section show that the average kinetic energy of the gap is very low in experimental situations of present concern ($k_B T\approx 10^{-4}$ eV for $T=1$ K and $N_e=10^6$ cm^{-2}) so that a 10-keV proton (or even a 100-eV one) easily fulfills the condition $V\gg V_{\text{th}}$.

ACKNOWLEDGMENTS

The Laboratoire de Physique des Gaz et des Plasmas is "associé au CNRS."

APPENDIX A

We proceed here to the calculation of the function f defined in Eq. (14)

$$f(x)=\lim_{\eta'\to 0}\int_0^\infty Q\eta^0(Q)dQ\int_0^{2\pi}\frac{d\theta}{x-Q\cos\theta+i\eta'} .$$

We first evaluate

$$g(x)=\frac{1}{x}\lim_{\eta'\to 0}\int_0^{2\pi}\frac{d\theta}{1-\frac{Q}{x}\cos\theta+i\frac{\eta'}{x}} .$$

One just has to take care about the sign of the quantity η'/x when using the Plemlej formula

$$\lim_{\varepsilon\to 0}\frac{1}{x\pm i\varepsilon}=\frac{1}{x}\mp i\pi\delta(x) .$$

We then have

$$R_e[g(x)]=\begin{cases}\frac{|x|}{x}\frac{2\pi}{\sqrt{x^2-q^2}} & \text{if } |x|>|q| \\ 0 \text{ otherwise,}\end{cases}$$

and

$$\text{Im}[g(x)]=\begin{cases}\frac{2\pi}{\sqrt{q^2-x^2}} & \text{if } |x|<|q| \\ 0 \text{ otherwise,}\end{cases}$$

which yields Eq. (15) of the main text

$$f(x)=2\pi\frac{x}{|x|}\int_0^x\frac{Qn^0(Q)dQ}{\sqrt{x^2-Q^2}}-2i\pi\int_x^\infty\frac{Qn^0(Q)dQ}{\sqrt{Q^2-x^2}} .$$

APPENDIX B

We here derive the result (54). Since $f_2(x,u=0)=0$, we may write from Eq. (48)

$$\varepsilon(z,u=0)=1-\frac{\pi\chi^2}{4z^2}f_1(z,u=0)$$

so that the left-hand side of Eq. (54) reads as

$$z-\frac{\chi^2}{4z}f_1(z,0)=z\varepsilon(z,u=0) .$$

Next, we evaluate the static response function $\varepsilon(z,u=0)$, getting

$$\varepsilon(z,u=0)=1+\frac{\pi\chi^2}{z^2}\int_0^z\frac{Qn^0(Q)}{(z^2-Q^2)^{1/2}}dQ .$$

One then can write

$$\varepsilon(z,u=0)=1+\frac{\pi\chi^2}{z^2}n^0(z\theta_z)\int_0^z\frac{Q}{(z^2-Q^2)^{1/2}}dQ ,$$

where $0<\theta_z<1$ so that

$$\varepsilon(z,u=0)=1+\frac{\pi\chi^2}{z^2}n^0(z\theta_z)z$$

and

$$\varepsilon(z\approx 0,u=0)\approx 1+\frac{\pi\chi^2}{z^2}n^0(0)$$

since $n^0(z\theta_z)\to n^0(0)$ when $z\to 0$ (because $0<\theta_z<1$). The result comes through Eq. (11) which indicates that

$$n^0(0)=\frac{1}{1+\exp\left[\frac{-\gamma}{T_e}\right]}=\frac{1}{1+\exp(-\alpha^e)} .$$

[1] A. L. Fetter, Phys. Rev. B **10**, 3739 (1974).
[2] F. Stern, Phys. Rev. Lett. **18**, 546 (1967).
[3] P. M. Platzman and N. Tzoar, Phys. Rev. B **13**, 3197 (1976).
[4] C. Gouédard and C. Deutsch, J. Math. Phys. **19**, 32 (1978).
[5] R. K. P. Zia, J. Phys. C **6**, 3121 (1973).
[6] P. Nozières, *Le Problème à N Corps* (Dunod, Paris, 1963), pp. 31–42.
[7] J. K. Lindhard, K. Dan. Vidensk. Selsk. Mat. Fys. Medd. **28**, No. 8 (1954)
[8] R. H. Ritchie, W. Brandt, and P. M. Echenique, Phys. Rev. B **14**, 4808 (1976).

[9] A. Bret and C. Deutsch, Phys. Rev. E **47**, 1276 (1993).
[10] G. Maynard and C. Deutsch, J. Phys. (Paris) **46**, 1113 (1985).
[11] T. Ando, A. B. Fowler, and F. Stern, Rev. Mod. Phys. **54**, 437 (1982).
[12] C. Deutsch, J. Stat. Phys. **32**, 115 (1983); Phys. Lett. **49A**, 40 (1983).
[13] E. Fermi, *Nuclear Physics* (The University of Chicago Press, Chicago, 1956), p. 27.